Journal of Alloys and Compounds 500 (2010) 39–45

Contents lists available at ScienceDirect

Journal of Alloys and Compounds

journal homepage: www.elsevier.com/locate/jallcom

Revisiting mechanisms to inhibit Ag_3Sn plates in Sn–Ag–Cu solders with 1 wt.% Zn addition

Z.-B. Luo, J. Zhao, Y.-J. Gao, L. Wang*

School of Materials Science and Engineering, Dalian University of Technology, Dalian 116024, PR China

ARTICLE INFO

Article history:
Received 12 January 2010
Received in revised form 19 March 2010
Accepted 25 March 2010
Available online 1 April 2010

Keywords:
Sn–Ag–Cu
Zn
Ag_3Sn
$(Cu,Ag)_5Zn_8$
Cooling rate

ABSTRACT

Two mechanisms to inhibit Ag_3Sn plates were discovered in Sn–1.0Ag–0.5Cu and Sn–3.0Ag–0.5Cu with 1 wt.% Zn addition. It was revealed that 1 wt.% Zn not only reduced the supercooling of β-Sn, but also promoted the formation of γ-$(Cu,Ag)_5Zn_8$ compounds. The amount of γ-$(Cu,Ag)_5Zn_8$ was larger in Sn–3.0Ag–0.5Cu than that in Sn–1.0Ag–0.5Cu. Meanwhile, the Ag content in γ-$(Cu,Ag)_5Zn_8$ was higher in the high-Ag solder. Although more γ particles formed under slow cooling rate, the Ag content varied a little with cooling rate.

1. Introduction

Sn–Ag–Cu alloys, as promising candidates for replacing the toxic Pb-bearing solders in surface mounting technology, have been widely accepted [1–3]. For example, Sn–3.0Ag–0.5Cu has become a standard solder in the electronic industry and Sn–1.0Ag–0.5Cu has been proved a superior resistance to drop failure [4]. However, some problems are still in suspense. As one case, the formation of large Ag_3Sn plates would cause heterogeneous distribution of stress and deteriorate the reliability of the solder joints [5,6].

In order to clarify the formation mechanisms and avoid large Ag_3Sn plates, a great deal of work has been carried out from different perspectives, such as solidification procedure, cooling rate, and Ag content [6–10]. It was revealed that Ag_3Sn plates nucleate and grow rapidly with minimal supercooling in the middle of the cooling stage. Sub-plates and directions with preferable growth were observed. At slow cooling, eutectic Ag_3Sn could boost the growth of primary Ag_3Sn crystals due to their matching crystalline orientation relationship. Sometimes, the plates can even extend to the whole solder joint in high-Ag solder.

The effects of alloying elements on Sn–Ag–Cu bulk solders have also been studied [8,11–13]. Inspiring results have been obtained. Zn was demonstrated to be one of the most effective elements. Kang et al. [8] found that with 0.1 wt.% Zn addition to Sn–Ag–Cu solder, the supercooling was reduced effectively to only a few centigrade degrees and large Ag_3Sn plates were inhibited. They suggested that Zn atoms preferentially react with Cu atoms and Cu–Zn intermetallic compound (IMC) form. Then it serves as the precursors to promote the nucleation of other phases. Besides, Kang et al. believed that 0.7 wt.% Zn had the similar effect on the supercooling. Interestingly, small Cu–Ag–Zn particles were observed in the EPMA mappings of Sn–Ag–Cu–0.7Zn solder, although they did not mention.

In Sn–Ag–Cu–Zn system, Zn can react with both Cu and Ag. Accompanying or following the formation of Cu–Zn, how Ag attends the reactions is still unclear. This is important to our better understanding about the mechanisms to inhibit Ag_3Sn plates. With low level Zn addition (e.g. 0.1 wt.%), however, it will be mainly consumed by the Cu element from both the bulk solder and the dissolution of substrate in solder joint. Thus, higher level Zn addition (e.g. 1 wt.%) is needed. Moreover, it was reported that the interfacial structure exhibited obvious change in Zn-containing solder joint under as-soldered and as-aged conditions [14,15]. The growth behavior of Cu_3Sn was influenced and Kirkendall voids at Cu/Cu_3Sn interface were suppressed [16]. It can provide a better reliability for the interconnects. To clarify the influence of Zn addition to Ag_3Sn plates and facilitate further study on solder joints, the solidification behaviors and microstructures of Sn–1.0Ag–0.5Cu and Sn–3.0Ag–0.5Cu with 1 wt.% Zn addition were investigated. Moreover, the distribution and content of Ag were analyzed comprehensively under furnace and air cooling conditions.

* Corresponding author. Tel.: +86 411 84707636; fax: +86 411 84709284.
E-mail address: wangl@dlut.edu.cn (L. Wang).

0925-8388/$ – see front matter © 2010 Elsevier B.V. All rights reserved.
doi:10.1016/j.jallcom.2010.03.191

Table 1
Composition analysis of as-received solder ingots with X-ray fluorescence (all in wt.%).

Solders	Sn	Ag	Cu	Zn	Si	Cr	Fe
SAC105	Balance	1.19	0.51	–	0.07	0.12	–
SAC105Z	Balance	1.11	0.52	1.05	0.15	0.15	–
SAC305	Balance	3.11	0.53	–	0.11	–	–
SAC305Z	Balance	3.12	0.50	1.10	0.12	0.12	0.07

2. Experimental procedures

Four alloys, Sn–1.0Ag–0.5Cu, Sn–1.0Ag–0.5Cu–1.0Zn, Sn–3.0Ag–0.5Cu and Sn–3.0Ag–0.5Cu–1.0Zn (wt.%, hereafter designated as SAC105, SAC105Z, SAC305 and SAC305Z, respectively) were prepared from high purity metals. They were melted in an argon atmosphere at 500 °C for several hours and then cooled down to room temperature in the furnace. Some ingots were selected as slow cooling samples. The others were re-melted at 270 °C for 20 min and then cast into a graphite mould which was pre-heated at 190 °C about an hour. The dimension of the as-cast ingot was 20 mm × 20 mm × 30 mm with a weight of about 90 g. To obtain a microstructure at the cooling rate similar to that of typical reflow oven and facilitate further analysis, the ingot was sectioned from the plane vertical to the 30 mm direction and 20 mm away from the shrinkage.

Owing to the chemically active nature of Zn, X-ray fluorescence analysis was conducted to confirm the composition of the as-received solder ingots, shown in Table 1. Only a trace amount of impurities were detected. The air cooling rate was determined with thermocouple inserted into the center of the liquid solder. The furnace cooling rate was the cooling profile of the atmosphere. By calculating the slope of the tangent to the curve at the start of solidification, 0.016 K/s for furnace cooling and 1.01 K/s for air cooling were obtained. Thermal behaviors of four kinds of solders were examined by differential scanning calorimetry (DSC) in argon atmosphere. The heating and cooling rate were 5 °C/min and the testing range was 180–260 °C. The microstructures were observed using optical microscope (OM) after all the samples were ground, polished and etched with a solution of 5 vol.% HNO_3–2 vol.% HCl–93 vol.% CH_3OH for several seconds. The compositions were identified using energy dispersive of X-ray (EDX) and electron probe microanalysis (EPMA). The phase structures were analyzed with X-ray diffraction (XRD).

3. Results

3.1. The effect of Zn addition on thermal properties

The heating and cooling curves of the solders are presented in Fig. 1. Peaks 1–6 are endothermal and the others are exothermic. The corresponding phase transformation temperatures are listed in Table 2. Obviously, the onsets of melting temperatures are nearly the same, ~217 °C, which corresponds to the eutectic transformation. So the effect of 1 wt.% Zn addition was minor. However, the temperatures of exothermic peaks varied a lot. By comparing the peak temperatures of eutectic reaction upon heating and cooling,

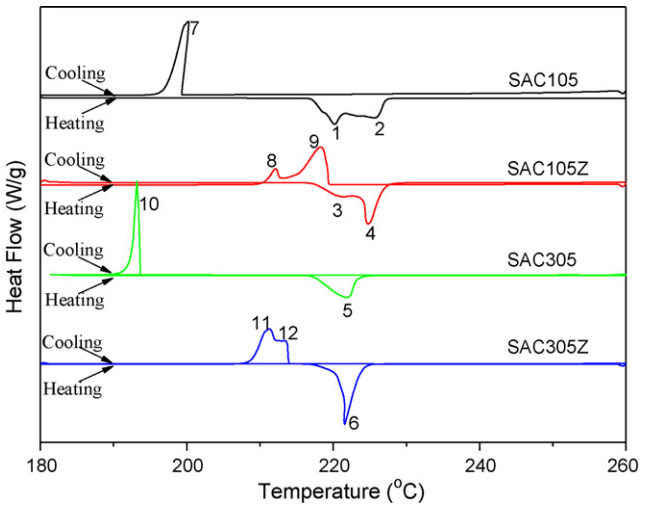

Fig. 1. DSC thermograms of solder alloys.

Table 2
Phase transformation temperatures in Fig. 1 and supercooling degree of four solder alloys (°C nos. in parentheses correspond to the peaks in Fig. 1).

Temperature	SAC105	SAC105Z	SAC305	SAC305Z
Onset	217.2	217.3	217.3	217.3
Heating peak	220.2 (1)	221.5 (3)	221.8 (5)	221.5 (6)
	226.1 (2)	224.9 (4)		
Cooling peak	199.8 (7)	211.7 (8)	193.2 (10)	211.5 (11)
		218.2 (9)		213.5 (12)
Supercooling degree	20.4	9.8	28.6	10

the supercooling was obtained as listed in Table 2. The values for SAC105 and SAC305 were 20.4 °C and 28.6 °C, respectively. With Zn addition, the degree of supercooling decreased to ~10 °C. At the same time, two peaks were observed in each cooling curve of Zn-containing solders. This indicates that Zn addition promoted the solidification of β-Sn, which corresponds to peaks 9 and 12. Subsequently, the eutectic reaction happened shown as peaks 8 and 11. As a result, the corresponding supercooling degrees were reduced, in accordance with the previously reported results [7,8,11,17].

3.2. The effect of Zn addition on microstructures

The air-cooling microstructures of four solders are shown in Fig. 2. Both SAC105 and SAC305 were composed of β-Sn and eutectic regions. However, the microstructures changed considerably after Zn addition as shown in Fig. 2(b) and (d). β-Sn dendrites were effectively refined and the fraction of eutectic region was increased. New IMC particles were also detected with the largest size about 10 μm. Composition analysis showed that the larger ones were Cu–Ag–Zn IMCs.

To examine the effect of slow cooling on the secondary phases, furnace cooling microstructures are given in Fig. 3. Coarsened IMCs were observed in all the samples. A few plate-like Ag_3Sn formed in SAC105 and the amount increased in SAC305, as depicted in Fig. 3(c). Whereas in Zn-containing solders revealed by Fig. 3(b) and (d), plate-like IMCs were seldom detected. Only a few small stripes and many circular IMCs were discovered. EDX results showed that they were Cu–Ag–Zn IMCs.

3.3. The formation of Cu–Ag–Zn compounds

EPMA mappings of Zn-containing solders are shown in Figs. 4 and 5 to confirm the composition of IMCs and element distribution. The corresponding elemental concentrations of IMCs are listed in Table 3. As revealed by spots 1 and 6 in Fig. 4 and 10–12 in Fig. 5, the Cu–Ag–Zn compounds always existed. The ratio for (Cu + Ag) to Zn was about 0.62–0.70, which is close to the stoichiometry of $(Cu,Ag)_5Zn_8$. Moreover, the Ag contents were ~9 at.% in SAC305Z and only ~2 at.% in SAC105Z. They were all independent of composition and cooling condition. Concurrently, Ag-rich Cu–Ag–Zn IMC was discovered at spot 7 which encircled $(Cu,Ag)_5Zn_8$. Its detailed composition approximated to $(Ag,Cu)_5Zn_8$. On the whole, higher amounts of $(Cu,Ag)_5Zn_8$ and Ag_3Sn were observed in the high-Ag solder, although no Ag_3Sn was discovered in furnace cooling SAC105Z due to the small amount. Only two kinds of IMCs were detected under furnace cooling, namely, Ag_3Sn and $(Cu,Ag)_5Zn_8$. In the case of air cooling, the secondary phases became complex. Some were present in the form of Sn–Ag–Cu–Zn and the detailed composition varied a lot. Most likely, they were mixture of different IMC particles.

XRD was conducted to identify the phase structures of Zn-containing solders and corresponding patterns are presented in Fig. 6. Because the spectra of SAC solders under different conditions

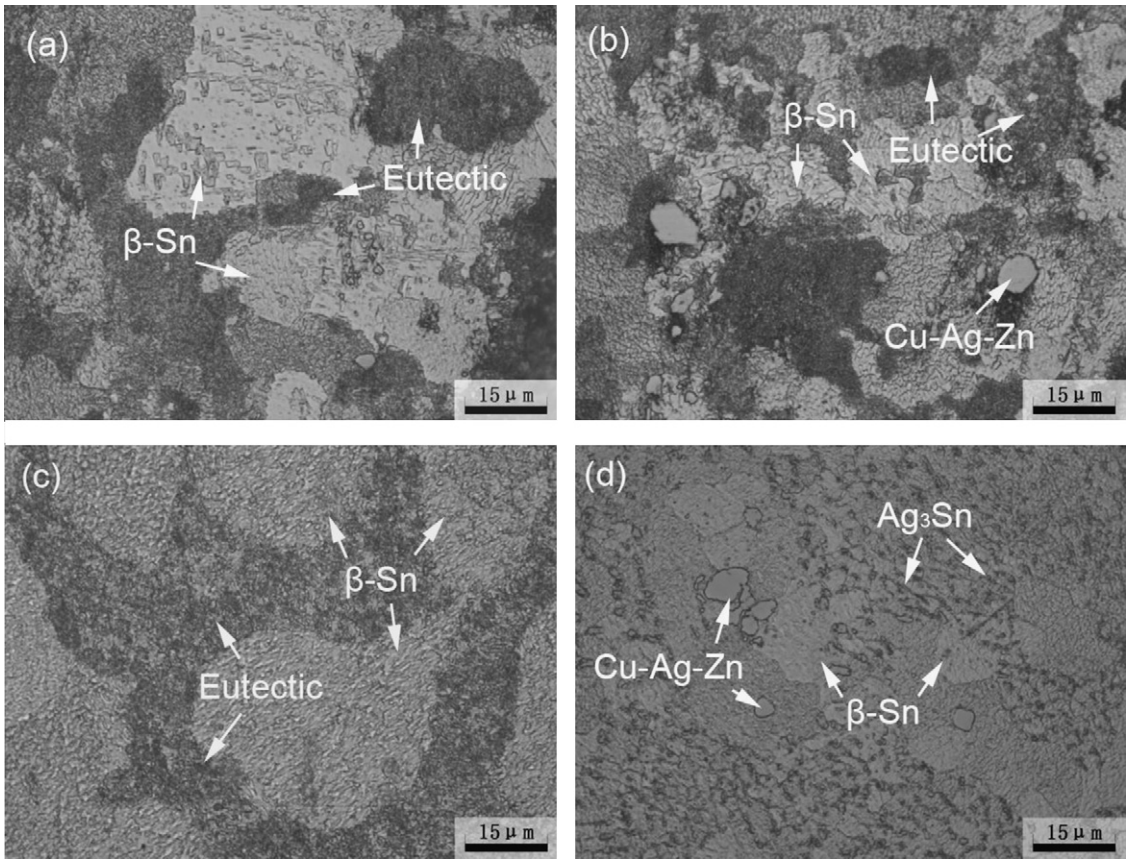

Fig. 2. Optical microstructures of four solders solidified under air cooling: (a) SAC105, (b) SAC105Z, (c) SAC305 and (d) SAC305Z.

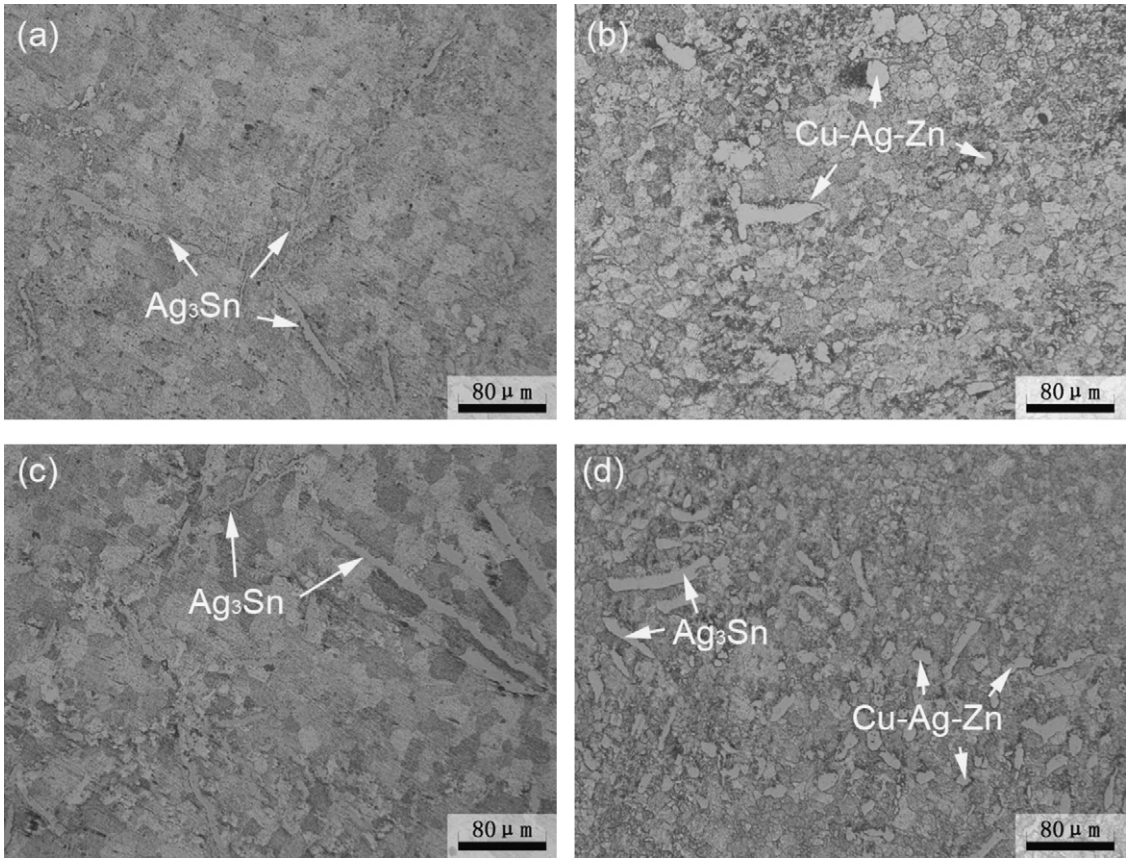

Fig. 3. Optical microstructures of four solders solidified under furnace cooling: (a) SAC105, (b) SAC105Z, (c) SAC305 and (d) SAC305Z.

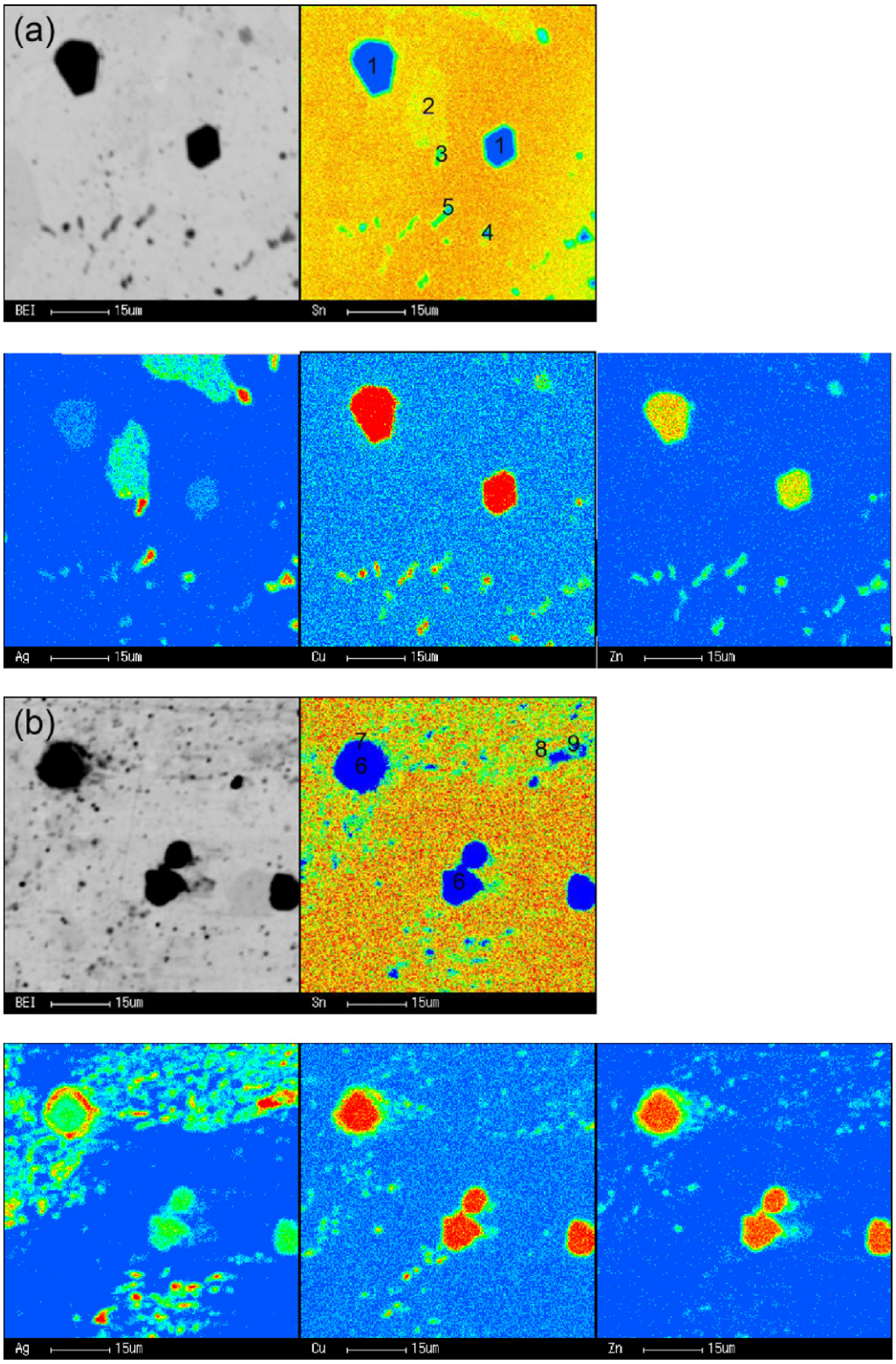

Fig. 4. EPMA mappings of Zn-containing solders under air cooling: (a) SAC105Z and (b) SAC305Z.

were similar to each other, only air cooling SAC305 was selected as a reference to avoid duplication. Stronger peaks of Ag_3Sn phase were observed in the high-Ag solders. Besides, it can be seen that γ-$(Cu,Ag)_5Zn_8$ formed and the peaks shifted to left a little, as indicated by arrows.

4. Discussion

Cooling rate, as a controllable environmental parameter, serves as an important factor on the solidification process. The cooling rate of typical reflow oven is about 1.0–4.0 K/s and it can reach

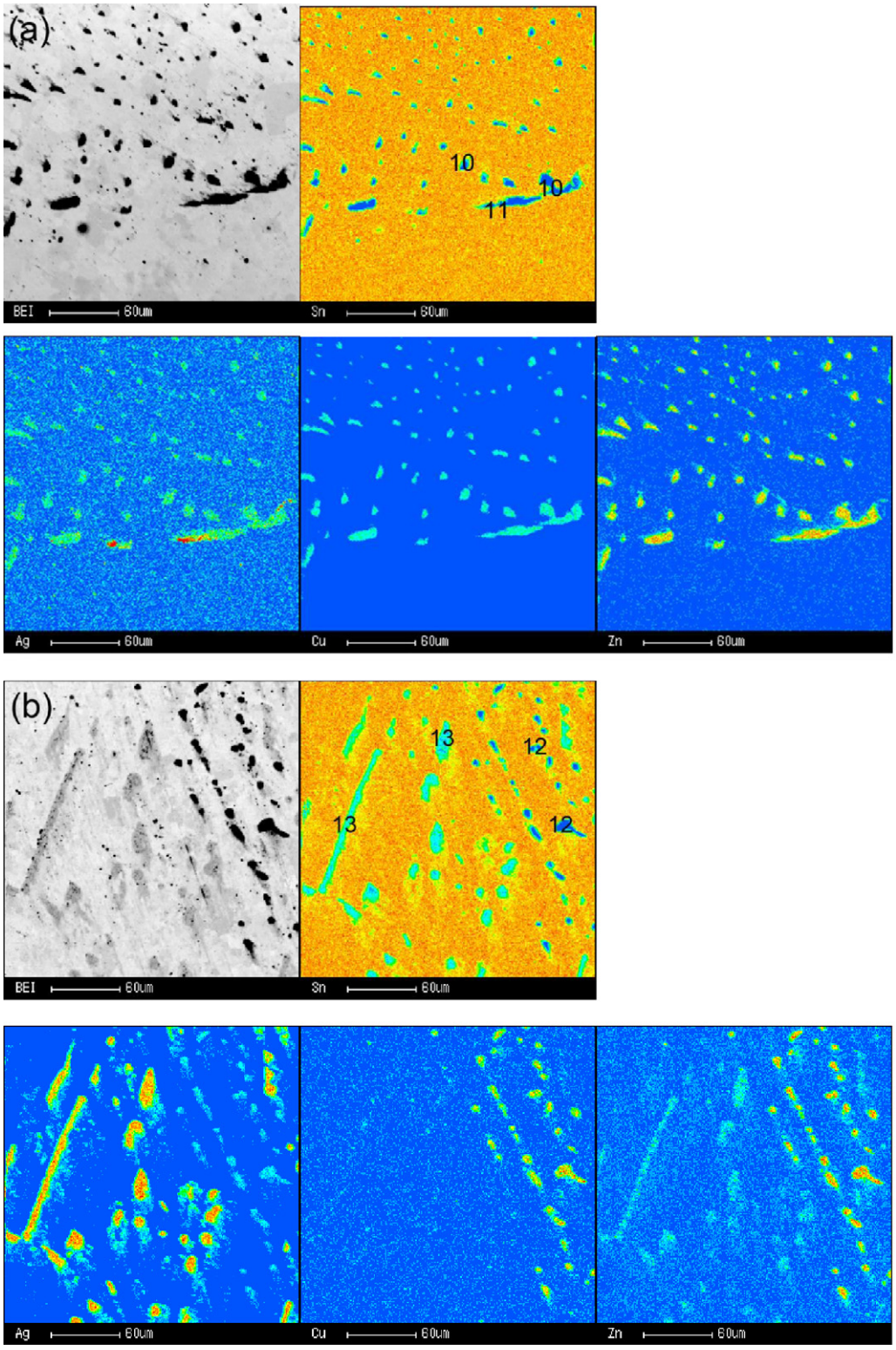

Fig. 5. EPMA mappings of Zn-containing solders under furnace cooling: (a) SAC105Z and (b) SAC305Z.

the level of 10^{-2} K/s under slow cooling in furnace. Due to the distinct supercooling degrees between β-Sn and Ag_3Sn [6,7], the microstructure of Sn–Ag–Cu is quite sensitive to the cooling rate, therefore raising worries about the reliabilities of interconnects. Fortunately, minor Zn brought SAC105Z and SAC305Z acceptable supercooling. As for the exact mechanisms, Kang et al. [8] suggested that Cu–Zn IMCs promote the nucleation of β-Sn. This is similar to the result of Gong et al. [18], who have studied the formation sequence of reactants in Sn–3.8Ag–0.7Cu/Cu. In Sn–Zn binary system, however, the surface of Zn has been demonstrated to be a preferable site for heterogeneous nucleation of β-Sn [17]. Although now we cannot make a conclusion which mechanism is dominant or both are critical in the multicomponent Sn-rich system, minor Zn addition to SAC solder decrease the supercooling effectively. At

Table 3
Elemental concentration of IMCs in Zn-containing solders (spot nos. correspond to those in Figs. 4 and 5).

Cooling profiles	Solders	Spots	Sn		Ag		Cu		Zn		IMC type
			w.t.%	mol.%	w.t.%	mol.%	w.t.%	mol.%	w.t.%	mol.%	
Air cooling	SAC105Z	1	1.8	1.0	2.7	1.7	36.2	37.5	59.3	59.8	$(Cu,Ag)_5Zn_8$
		2	93.8	93.1	6.0	6.5	0	0	0.2	0.4	Sn–Ag
		3	28.0	26.0	71.6	73.3	0	0	0.4	0.7	Ag_3Sn
		4	53.9	45.3	26.6	24.6	5.1	8.1	14.4	21.9	$(Cu,Ag)_5Zn_8$ and Ag_3Sn
		5	34.0	27.3	41.3	36.6	3.7	5.5	21.0	30.6	$(Cu,Ag)_5Zn_8$ and Ag_3Sn
	SAC305Z	6	2.3	1.3	14.6	9.4	27.7	30.4	55.3	58.9	$(Cu,Ag)_5Zn_8$
		7	3.1	2.0	33.0	23.1	15.2	18.1	48.6	56.8	$(Ag,Cu)_5Zn_8$
		8	25.4	23.4	72.9	74.0	0.8	1.4	1.0	1.6	$(Ag,Zn)_3Sn$
		9	36.1	29.8	43.8	39.8	3.7	5.7	16.5	24.7	$(Cu,Ag)_5Zn_8$ and Ag_3Sn
Furnace cooling	SAC105Z	10	1.0	0.5	3.2	1.9	35.0	36.2	61.0	61.3	$(Cu,Ag)_5Zn_8$
		11	4.9	2.9	12.2	8.1	26.9	30.1	54.2	58.9	$(Cu,Ag)_5Zn_8$
	SAC305Z	12	2.6	1.6	13.6	9.0	28.1	31.61	52.7	57.8	$(Cu,Ag)_5Zn_8$
		13	22.0	22.3	62.9	70.0	0.4	0.81	3.7	6.9	$(Ag,Zn)_3Sn$

this point of view, it can inhibit the formation of coarsened Ag_3Sn plates.

Cu–Ag–Zn IMC is the main concern in this work. Both Ag and Cu atoms can react with Zn to form IMCs, such as ξ-AgZn, γ-Ag_5Zn_8, ε-$AgZn_3$, γ-Cu_5Zn_8. It has been confirmed by experiments and calculations that γ-Cu_5Zn_8 was preferred due to the larger driving force [19,20]. Accompanying the consumption of Cu in the interaction with Zn, Ag would serve as substituting atoms. Thus, γ phase grew with high-Ag content. Remembering that the atomic radii of Cu and Ag are 1.57 Å and 1.75 Å respectively, the distance of crystal plane will increase with Cu atoms substituted. So the corresponding peaks in XRD spectrum shifted to left as shown in Fig. 6. No relative information about Sn–Ag–Cu–Zn quaternary IMCs has come to our knowledge among phase diagrams and literatures. Illumined by the IMC shape at spots 5–7 in Fig. 4, we believe that they were the mixture of γ phase and Ag_3Sn. Driven by the large Gibbs free energy change [19,20], γ phase forms first and provides preferable nucleation sites to Ag_3Sn.

It is interesting that the amount and the Ag content of γ-$(Cu,Ag)_5Zn_8$ are both different in two Zn-containing solders. Some researchers suggested that it might be related to the medium range order structure [21,22]. Concretely, 3 wt.% Ag in SAC305Z would promote the formation of γ-$(Cu,Ag)_5Zn_8$ and more Ag atoms will replace Cu atoms in the lattice. On one hand, Ag has a relatively high solubility limit in Cu_5Zn_8, about 43 at.% [23]. On the other hand, more γ particles formed in the high-Ag solder. This means that there would be more capacity to accommodate additional Ag atoms and the corresponding formation of Ag_3Sn would be reduced. This is proposed as the second effect of 1 wt.% Zn addition to SAC solders to inhibit the formation of Ag_3Sn plates.

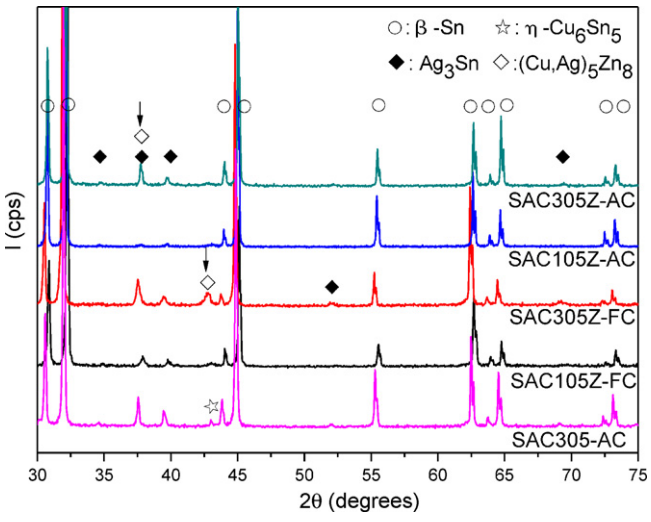

Fig. 6. XRD patterns of solders under air cooling (AC) and furnace cooling (FC).

The results of Kang et al. indicated that 0.1 wt.% and 0.7 wt.% Zn inhibited the supercooling of Sn–Ag–Cu solder. Moreover, Cu–Ag–Zn formed with 0.7 wt.% Zn addition [8]. Combined with this study, it is reasonable to make conclusions that the formation of γ phase relies on the content of Zn in bulk solder. The mechanisms of Zn addition to inhibit Ag_3Sn plates in SAC solders vary with the content of Zn: at minute content, e.g. 0.1 wt.%, reducing the supercooling of β-Sn is exclusive; at a little higher content, e.g. 0.7 wt.% or more, the Cu–Ag–Zn IMCs is also another important aspect.

5. Conclusions

Sn–1.0Ag–0.5Cu and Sn–3.0Ag–0.5Cu with 1 wt.% Zn addition were investigated with different cooling rates, i.e., furnace and air cooling. The aim is to explore the mechanisms of Zn addition on the formation of Ag_3Sn plates. The important results are summarized as follows:

(1) 1 wt.% Zn not only reduced the supercooling of β-Sn, but also promoted the formation of γ-$(Cu,Ag)_5Zn_8$. The γ phase played a role in accommodating additional Ag atoms, which is beneficial to inhibit Ag_3Sn plates.
(2) The amount of γ-$(Cu,Ag)_5Zn_8$ was larger in SAC305Z than that in SAC105Z solder. Slow cooling also promoted the formation of γ phase. Simultaneously, the Ag contents in γ-$(Cu,Ag)_5Zn_8$ were higher in SAC305Z solder and they varied a little with cooling rate.

Acknowledgment

This work has been supported by the National Key Project of Scientific and Technical Supporting Programs during the 11th Five-Year Plan (No. 2006BAE03B02-2).

References

[1] D.Q. Yu, L. Wang, J. Alloys Compd. 458 (2008) 542–547.
[2] S.Y. Chang, Y.C. Huang, Y.M. Lin, J. Alloys Compd. 490 (2010) 508–514.
[3] X.Y. Liu, M.L. Huang, Y.H. Zhao, C.M.L. Wu, L. Wang, J. Alloys Compd. 492 (2010) 433–438.
[4] D. Suh, D.W. Kim, P. Liu, H. Kim, J.A. Weninger, C.M. Kumar, A. Prasad, B.W. Grimsley, H.B. Tejada, Mater. Sci. Eng. A 460–461 (2007) 595–603.
[5] K.S. Kim, S.H. Huh, K. Sugannuma, J. Alloys Compd. 352 (2003) 226–236.
[6] D.W. Henderson, T. Gosselin, A. Sarkhel, S.K. Kang, W.K. Choi, D.Y. Shih, C. Goldsmith, K.J. Puttlitz, J. Mater. Res. 17 (2002) 2775–2778.

[7] S.K. Kang, W.K. Choi, D.Y. Shih, D.W. Henderson, T. Gosselin, A. Sarkhel, C. Goldsmith, K.J. Puttlitz, JOM 55 (2003) 61–65.
[8] S.K. Kang, D.Y. Shih, D. Leonard, D.W. Henderson, T. Gosselin, S. Cho, J. Yu, W.K. Choi, JOM 56 (2004) 34–38.
[9] J. Shen, Y.C. Chan, S.Y. Liu, Intermetallics 16 (2008) 1142–1148.
[10] J.C. Gong, C.Q. Liu, P.P. Conway, V.V. Silberschmidt, Mater. Sci. Eng. A 527 (2010) 2588–2591.
[11] J.M. Song, C.F. Huang, H.Y. Chuang, J. Electron. Mater. 35 (2006) 2154–2163.
[12] M. McCormack, G.W. Kammlott, H.S. Chen, S. Jin, Appl. Phys. Lett. 65 (1994) 1233–1235.
[13] F.J. Cheng, F. Gao, H. Nishikawa, T. Takemoto, J. Alloys Compd. 472 (2009) 530–534.
[14] F.J. Wang, Z.S. Yu, K. Qi, J. Alloys Compd. 438 (2007) 110–115.
[15] J. Chen, J. Shen, S.Q. Lai, D. Min, X.C. Wang, J. Alloys Compd. 489 (2010) 631–637.
[16] M.Y. Tsai, S.C. Yang, Y.W. Wang, C.R. Kao, J. Alloys Compd. 494 (2010) 123–127.
[17] M.G. Cho, H.Y. Kim, S.K. Seo, H.M. Lee, Appl. Phys. Lett. 95 (2009) 021905.
[18] J.C. Gong, C.Q. Liu, P.P. Conway, V.V. Silberschmidt, Scripta Mater. 61 (2009) 682–685.
[19] S.W. Yoon, J.R. Soh, H.M. Lee, B.J. Lee, Acta Mater. 45 (1997) 951–960.
[20] B.J. Lee, N.M. Hwang, H.M. Lee, Acta Mater. 45 (1997) 1867–1874.
[21] X.F. Bian, X.M. Pan, X.B. Qin, M.H. Jiang, Sci. China E 32 (2002) 145–151.
[22] N. Zhao, X.M. Pan, H.T. Ma, L. Wang, Acta Metall. Sin. 44 (2008) 467–472.
[23] R. Hultgren, R.L. Orr, P.D. Anderson, K.K. Kelley, Selective Values of Thermodynamics Properties of Metals and Alloys, John Willey & Sons, Inc., New York, 1990.